

# Efficient Shape Optimization via Parametric Model Embedding

A. Serani\* and M. Diez†

CNR-INM, National Research Council-Institute of Marine Engineering, Rome, Italy

D. Quagliarella‡

CIRA, Italian Aerospace Research Centre, Capua (CE), Italy

The search for unconventional and highly innovative shape designs via simulation-based design optimization (SBDO) still remains a difficult task. Furthermore, the tendency is to define ever larger design space, which collides with the well-known curse of dimensionality problem. Representation learning methods represent a viable option in this context, nevertheless currently available techniques are not able to explicitly reconstruct the original parameterization, representing a limitation to their widespread use in the industrial field, where the design parameters often pertain to well-established parametric CAD models. This work presents a new methodology, recently developed by the authors and called parametric model embedding (PME), for efficiently and effectively solve SBDO problems. The methodology is capable of reducing the dimensionality of the design space and, at the same time, providing an explicit relationship with the original parameterization. The capabilities of the PME are shown for the optimization of a naval destroyer model, the DTMB 5415, in calm water and an airfoil, the RAE 2822, in transonic conditions.

## I. Introduction

Despite the enormous development, in the last decade, of the available computational capabilities, shape design, driven by increasingly specific and complex requirements, still remains a difficult task, especially when it is based on high-fidelity computational solvers. Furthermore, in the search for excellent unconventional and highly innovative designs, the tendency is to define ever larger design spaces. This collides, in the world of global optimization, with the well-known phenomenon of the *curse of dimensionality* [1], whereby the performance of an optimization algorithm, as well as the training of a surrogate model, degrades with the increase of the dimensionality of the design space. For this reason, specially in industrial design, where time resources are generally limited, techniques for reducing the computational burden of simulation-based design optimization (SBDO) [2] and in particular for the reduction of the design space, before the optimization process, capable of describing with a certain degree of accuracy the variability of the original space, are strictly necessary.

The simplest methodology to reduce the dimensionality of the design space is to identify the most important variables for the design problem and discard the remaining ones by setting them to a constant value during the optimization process, i.e. a factor screening [3]. This approach does not always provide the best solution, as it is not able to evaluate the importance that the fixed variables could have during the optimization process, especially when combined with other variables, which can be assessed by variance-based sensitivity analysis, i.e. using the Sobol indices [4]. Nevertheless, Sobol indices work in a probabilistic framework and consequently needs a statistically significant number of design-space samples. Furthermore, the number of indices increase with the power of the design-space dimensionality, so Sobol indices are generally computationally expensive.

Representation learning methods [5], capable of learning relevant hidden structures of the original design-space parameterization, represent a valid option in this context. A method based on the Karhunen-Loève expansion (KLE, equivalent to the proper orthogonal decomposition, POD) has been formulated in [6] for the assessment of the shape modification variability and the definition of a reduced-dimensionality global model of the shape modification vector. No objective function evaluation nor gradient is required by the method. The KLE is applied to the continuous shape modification vector and, once the equations are discretized, the problem reduces to the principal component analysis (PCA) of discrete geometrical data. The method improves the shape optimization efficiency by reparameterization and dimensionality reduction, providing the assessment of the design space and the shape parametrization before

\*Research Scientist, INM Rome, Via di Vallerano 139, 00128, AIAA Member. Email: andrea.serani@cnr.it

†Senior Research Scientist, INM Rome, Via di Vallerano 139, 00128, AIAA Member. Email: matteo.diez@cnr.it

‡Senior Research Scientist, CIRA, Via Maiorise, 81043. Email: d.quagliarella@cira.it

optimization and/or performance analysis are carried out. This method and closely related approaches, also known as modal parameterization [7], have been successfully applied for the solution of SBDO problems in aerodynamics of airfoils [8–10], wings [11], rotor blades [12], hydrodynamics of marine propellers [13], hydropower turbine [14], hull-forms [15–19], as well as to optics [20, 21]. Although their capacity to reduce design space is almost well known, currently available techniques are not able to explicitly reconstruct the original parameterization and solve the so-called *pre-image problem* [22]. This represents a limit for their extended use in the industrial context, as it obliges the user to use and implement a shape modification method based on the reduced parameterization, while the use of the original parameterization remains preferable, since it may have a well-known geometric meaning to the designer.

The present work presents a new methodology recently developed by the authors and called parametric model embedding (PME) [23], for the efficiency of shape optimization processes. The methodology is capable of reducing the dimensionality of the design space and, at the same time, providing an explicit relationship with the original settings. PME extends the formulation presented in [6] using a generalized feature space that includes shape modification and design variables vectors together with a generalized inner product, aiming at resolving a prescribed design variability by properly selecting the latent dimensionality.

The capabilities of PME are shown for the design-space reparameterization and the consequent solution of two single-objective SBDO problems pertaining to the shape optimization of a destroyer-type vessel in calm water and an airfoil in transonic conditions, by means of potential flow and Reynolds-averaged Navier-Stokes (RANS) solvers, respectively. Specifically, the hydrodynamic optimization of the DTMB 5415 model and aerodynamics of the RAE-2822 airfoil are used as test case.

## II. Dimensionality Reduction in Shape Optimization via Representation Learning

Consider a manifold  $\mathcal{G}$ , which identifies the original/parent shape, whose coordinates in the  $n$ D-space are represented by  $\mathbf{g}(\xi) \in \mathbb{R}^n$  with  $n = 1, 2$ , or 3;  $\xi \in \mathcal{G}$  are curvilinear coordinates defined on  $\mathcal{G}$ . Assume that, for the purpose of shape optimization,  $\mathbf{g}$  can be transformed to a deformed shape/geometry  $\mathbf{g}'(\xi, \mathbf{u})$  by

$$\mathbf{g}'(\xi, \mathbf{u}) = \mathbf{g}(\xi) + \delta(\xi, \mathbf{u}) \quad \forall \xi \in \mathcal{G} \quad (1)$$

where  $\delta(\xi, \mathbf{u}) \in \mathbb{R}^n$  is the resulting shape modification vector, defined by arbitrary shape parameterization or modification method (e.g., CAD parameterization, Bezier surfaces, FFD, NURBS, etc.), and  $\mathbf{u} \in \mathcal{U} \subset \mathbb{R}^M$  is the design variable vector. Figure 1 shows an example of the current notation for  $n = 2$ .

Consider, temporarily, the identification of the optimal design, through a SBDO optimization problem

$$\underset{\mathbf{u} \in \mathcal{U}}{\text{minimize}} \quad f(\mathbf{u}) \quad (2)$$

as a problem affected by epistemic uncertainty, where  $\mathbf{u}$  can be assumed as an uncertain/random parameter. The idea is that the optimal design exists but, before going through the optimization procedure, is unknown. Accordingly, the

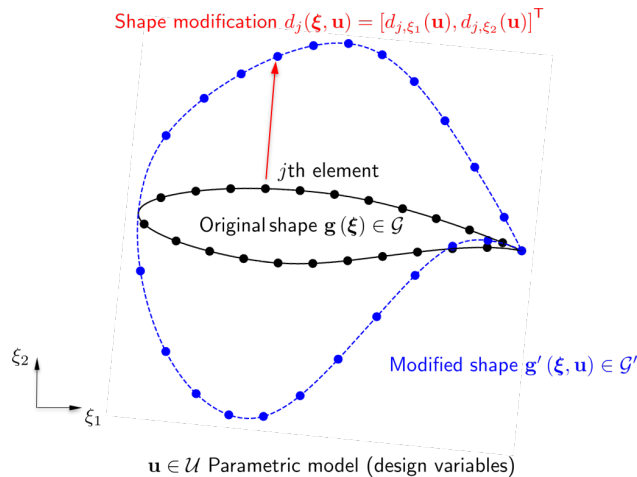


**Fig. 1** Shape modification example and notation for  $n = 2$

design variable vector  $\mathbf{u}$  is assigned with a probability density function (PDF)  $p(\mathbf{u})$ , representing the degree of belief in finding the optimal solution in a certain region of the design space.

Once  $p(\mathbf{u})$  is defined, the shape modification vector  $\delta$  goes stochastic and can be studied as a random field, e.g., by using the KLE, as representation learning approach.

#### A. Karhunen-Loëve expansion: dimensionality reduction in the continuum geometric space

Consider  $\delta(\xi, \mathbf{u})$  as belonging to a Hilbert space  $L^2_\rho(\mathcal{G})$ , defined by the generalized inner product

$$(\mathbf{a}, \mathbf{b})_\rho = \int_{\mathcal{G}} \rho(\xi) \mathbf{a}(\xi) \cdot \mathbf{b}(\xi) d\xi \quad (3)$$

with associated norm  $\|\mathbf{a}\| = (\mathbf{a}, \mathbf{a})_\rho^{1/2}$ , where  $\rho(\xi) \in \mathbb{R}$  is an arbitrary weight function. Consider all possible realization of  $\mathbf{u}$ , the associated mean vector of  $\delta$  is

$$\langle \delta \rangle = \int_{\mathcal{U}} \delta(\xi, \mathbf{u}) p(\mathbf{u}) d\mathbf{u} \quad (4)$$

and the associated geometrical variance equals to

$$\sigma^2 = \langle \|\hat{\delta}\|^2 \rangle = \iint_{\mathcal{U}, \mathcal{G}} \rho(\xi) \hat{\delta}(\xi, \mathbf{u}) \cdot \hat{\delta}(\xi, \mathbf{u}) p(\mathbf{u}) d\xi d\mathbf{u} \quad (5)$$

where  $\hat{\delta} = \delta - \langle \delta \rangle$ , with  $\langle \cdot \rangle$  the ensemble average obtained integrating  $\mathbf{u}$  over  $\mathcal{U}$ .

The aim of KLE is to find an optimal basis of orthonormal functions for the linear representation of  $\hat{\delta}$ :

$$\hat{\delta}(\xi, \mathbf{u}) \approx \sum_{k=1}^N x_k(\mathbf{u}) \phi_k(\xi) \quad (6)$$

where

$$x_k(\mathbf{u}) = (\hat{\delta}, \phi_k)_\rho = \int_{\mathcal{G}} \rho(\xi) \hat{\delta}(\xi, \mathbf{u}) \cdot \phi_k(\xi) d\xi \quad (7)$$

are the basis-function components usable as new (reduced) design variables. The optimality condition associated to the KLE refers to the geometric variance retained by the basis functions through Eq. 6. Combining Eqs. 5-7 yields

$$\sigma^2 = \sum_{k=1}^{\infty} \left\langle \left( \hat{\delta}, \phi_k \right)_\rho^2 \right\rangle \quad (8)$$

The basis retaining the maximum variance is formed by those  $\phi$ , solutions of the variational problem

$$\begin{aligned} & \underset{\phi \in L^2_\rho(\mathcal{G})}{\text{maximize}} \quad \mathcal{J}(\phi) = \left\langle \left( \hat{\delta}, \phi_k \right)_\rho^2 \right\rangle \\ & \text{subject to} \quad (\phi, \phi)_\rho^2 = 1 \end{aligned} \quad (9)$$

which yields [6]

$$\mathcal{L}\phi(\xi) = \int_{\mathcal{G}} \rho(\xi') \langle \hat{\delta}(\xi, \mathbf{u}) \otimes \hat{\delta}(\xi', \mathbf{u}) \rangle \phi(\xi') d\xi' = \lambda \phi(\xi) \quad (10)$$

where  $\otimes$  indicates the outer product and  $\mathcal{L}$  is the self-adjoint integral operator whose eigensolutions define the optimal basis functions for the linear representation of Eq. 6. Therefore, its eigenfunctions (KL-modes)  $\{\phi_k\}_{k=1}^{\infty}$  are orthonormal and form a complete basis for  $L^2_\rho(\mathcal{G})$ . Additionally, it may be proven that

$$\sigma^2 = \sum_{k=1}^{\infty} \lambda_k \quad \text{with} \quad \lambda_k = \langle x_k^2 \rangle \quad (11)$$

where the eigenvalues  $\lambda_k$  represent the variance retained by the associated basis function  $\phi_k$ , through its component  $x_k$ . Finally, the solution  $\{\phi_k\}_{k=1}^{\infty}$  of Eq. 9 are used to build a reduced dimensionality representation of the original design space; defining the desired confidence level  $l$ , with  $0 < l \leq 1$ , the number of reduced design variables  $N$  in Eq. 6 is selected such as

$$\sum_{k=1}^N \lambda_k \geq l \sum_{k=1}^{\infty} \lambda_k = l\sigma^2 \quad \text{with} \quad \lambda_k \geq \lambda_{k+1} \quad (12)$$

## B. Principal component analysis: dimensionality reduction in the discretized geometric space

Discretizing  $\mathcal{G}$  by  $L$  elements of measure  $\Delta\mathcal{G}_j$  (with  $j = 1, \dots, L$ ), sampling  $\mathcal{U}$  by a statistically convergent number of Monte Carlo (MC) realizations  $S$ , so that  $\{\mathbf{u}_k\}_{k=1}^S \sim p(\mathbf{u})$ , and organizing the discretization  $\hat{\mathbf{d}}(\xi, \mathbf{u}_k)$  of  $\hat{\delta}(\xi, \mathbf{u}_k)$  in a data matrix  $\mathbf{D}$  of dimensionality  $[nL \times S]$

$$\mathbf{D} = \begin{bmatrix} \hat{d}_{1,\xi_1}(\mathbf{u}_1) & \hat{d}_{1,\xi_1}(\mathbf{u}_S) \\ \vdots & \vdots \\ \hat{d}_{L,\xi_1}(\mathbf{u}_1) & \hat{d}_{L,\xi_1}(\mathbf{u}_S) \\ \vdots & \dots & \vdots \\ \hat{d}_{1,\xi_n}(\mathbf{u}_1) & \hat{d}_{1,\xi_n}(\mathbf{u}_S) \\ \vdots & \vdots \\ \hat{d}_{L,\xi_n}(\mathbf{u}_1) & \hat{d}_{L,\xi_n}(\mathbf{u}_S) \end{bmatrix} \quad (13)$$

where  $\hat{d}_{j,\xi_k}$  is the  $k$ -th component of the shape modification vector associated to the  $j$ -th element, the integral problem of Eq. 9 reduces to the generalized PCA of the data matrix  $\mathbf{D}$ , as follows

$$\mathbf{AGWZ} = \mathbf{Z}\Lambda \quad \text{with} \quad \mathbf{A} = \frac{1}{S}\mathbf{DD}^\top \quad (14)$$

where  $\mathbf{Z}$  and  $\Lambda$  are the eigenvectors and eigenvalues matrices of  $\mathbf{AGW}$ . Further details on the discretization process of the problem 10 and how it yields problem 14 can be found in [6]. The matrix  $\mathbf{G} = \text{diag}(\mathbf{G}_1, \dots, \mathbf{G}_n)$  is block diagonal and has dimensionality  $[nL \times nL]$ , with each  $[L \times L]$   $k$ -th block being a diagonal matrix itself

$$\mathbf{G}_k = \text{diag}(\Delta\mathcal{G}_1, \dots, \Delta\mathcal{G}_L) \quad (15)$$

containing the measure  $\Delta\mathcal{G}_j$  of the  $j$ -th element. Similarly,  $\mathbf{W} = \text{diag}(\mathbf{W}_1, \dots, \mathbf{W}_n)$  is a block diagonal matrix of dimensionality  $[nL \times nL]$ , where each  $[L \times L]$   $k$ -th block  $\mathbf{W}_k$  ( $k = 1, \dots, n$ ) is itself a diagonal matrix defined as

$$\mathbf{W}_k = \text{diag}(\rho_1, \dots, \rho_L) \quad (16)$$

with  $\rho_j$  (for  $j = 1, \dots, L$ ) the arbitrary weight given to each element.

Finally, note that for problems 14 the matrix  $\mathbf{Z}$  contains the discrete representation  $\mathbf{z}_k$  of the desired eigenfunctions  $\phi_k$ .

## III. Parametric Model Embedding

The design-space dimensionality reduction via KLE/PCA as already shown its capability in reducing the design-space dimensionality before the optimization loop, alleviating the CoD associated with the optimization problem [24]. Nevertheless, if the dimensionality reduction procedure is fed only with information on the shape modification vector, the method does not directly provide a way to return to the original design variables from the so-called latent space (the reduced dimensionality representation of the original shape parameterization). Two significant criticalities ensue: (1) shape modification-based KLE obliges the user to implement a new shape modification method based on the eigenfunctions  $\phi_k$ ; (2) moreover, depending on the bounds applied to the reduced design variables  $\mathbf{x}$ , there is not guarantee that the shape produced using KLE eigenvectors actually belongs to the original design space, thus potentially resulting in design unfeasibilities.

In order to overcome these limitations, starting from the discrete formulation presented in Section II.B, the data matrix  $\mathbf{D}$  used for the dimensionality reduction procedure is augmented with the values of design parameters from the original parameterization, as conceptually shown in Fig. 2.

Practically, defining  $\hat{\mathbf{u}} = \mathbf{u} - \langle \mathbf{u} \rangle$ , the embedding is achieved introducing a new matrix  $\mathbf{P}$  of dimensionality  $[(nL + M) \times S]$  as follows

$$\mathbf{P} = \begin{bmatrix} \mathbf{D} \\ \mathbf{U} \end{bmatrix} \quad \text{with} \quad \mathbf{U} = \begin{bmatrix} \hat{u}_{1,1} & \hat{u}_{1,S} \\ \vdots & \dots & \vdots \\ \hat{u}_{M,1} & \hat{u}_{M,S} \end{bmatrix} \quad (17)$$

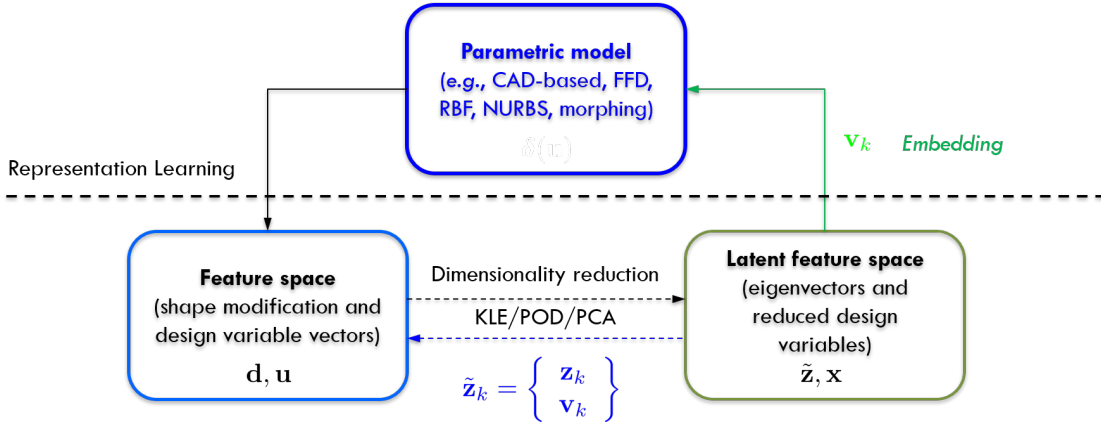


**Fig. 2** Parametric model embedding concept

where the matrix  $\mathbf{U}$  is added to the data matrix  $\mathbf{D}$  with a null weight  $\mathbf{W}_u$  such that

$$\mathbf{W}_u = \mathbf{0} \quad \text{and} \quad \widetilde{\mathbf{W}} = \begin{bmatrix} \mathbf{W} & \mathbf{0} \\ \mathbf{0} & \mathbf{W}_u \end{bmatrix} \quad (18)$$

and so recasting Eq. 14 to

$$\widetilde{\mathbf{A}}\widetilde{\mathbf{G}}\widetilde{\mathbf{W}}\widetilde{\mathbf{Z}} = \widetilde{\mathbf{Z}}\widetilde{\Lambda} \quad \text{with} \quad \widetilde{\mathbf{A}} = \frac{1}{S}\mathbf{P}\mathbf{P}^T \quad (19)$$

where

$$\widetilde{\mathbf{G}} = \begin{bmatrix} \mathbf{G} & \mathbf{0} \\ \mathbf{0} & \mathbf{I} \end{bmatrix} \quad \text{and} \quad \widetilde{\mathbf{Z}} = [\tilde{\mathbf{z}}_1 \dots \tilde{\mathbf{z}}_S] \quad \text{with} \quad \tilde{\mathbf{z}}_k = \begin{Bmatrix} \mathbf{z}_k \\ \mathbf{v}_k \end{Bmatrix} \quad (20)$$

Having given a null weight to  $\mathbf{U}$  does not remove the contribution of the design variables from the inner product, but just cancels as many columns as  $M$  from the matrix  $\widetilde{\mathbf{A}}\widetilde{\mathbf{G}}\widetilde{\mathbf{W}}$ , thus Eqs. 14 and 20 provides the same eigenvalues ( $\Lambda = \widetilde{\Lambda}$ ) and geometrical components of the eigenvectors ( $\mathbf{z}_k$ , except for a multiplicative constant). The proof of the equivalence between KLE and PME can be found in [23]. In addition and as desired, the solution of Eq. 20 provides the eigenvector components  $\mathbf{v}_k$  that embeds the original design variables  $\mathbf{u}$ .

In order to reconstruct at least all the samples in  $\mathbf{D}$ , the reduced design variables  $\mathbf{x}$  are bounded such as  $\inf\{\beta_k\} \leq \mathbf{x} \leq \sup\{\beta_k\}$ , with

$$\beta_k = \mathbf{p}_k^T \widetilde{\mathbf{G}} \widetilde{\mathbf{W}} \widetilde{\mathbf{Z}}' \quad \text{for } k = 1, \dots, S \quad (21)$$

where  $\widetilde{\mathbf{Z}}'$  contains only the first  $N$  eigenvectors of  $\widetilde{\mathbf{Z}}$ , retaining the desired level of variance of the original design space, and  $\mathbf{p}_k$  is a column of the matrix  $\mathbf{P}$ .

The PME of the original design variables is finally achieved by

$$\mathbf{u} \approx \check{\mathbf{u}} = \langle \mathbf{u} \rangle + \sum_{k=1}^N x_k \mathbf{v}_k \quad (22)$$

where the eigenvectors component  $\mathbf{v}_k$  embeds (or contains) the reduced-order representation of the original design parameterization. It may be noted that the overall methodology is independent from the specific shape modification method, which is seen as a black box by PME.

#### IV. Ship Hydrodynamics Problem

The problem assess the shape reparameterization and optimization of the DTMB 5415 model, an open-to-public naval combatant widely used as benchmark in the ship hydrodynamic community [25]. The PME effectiveness is shown

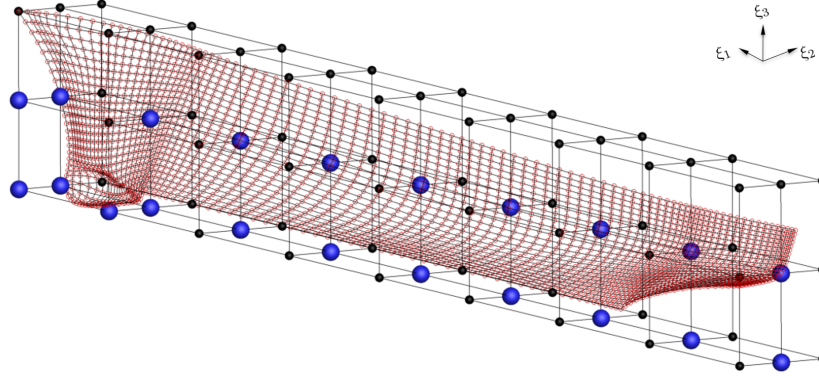


**Fig. 3 DTMB 5415 problem: FFD design space definition and grid nodes used for the dimensionality reduction**

for the solution of a SDDO formulated as follows

$$\begin{aligned}
 & \text{minimize} && R(\mathbf{u}) \\
 & \text{subject to} && L_{\text{pp}} = L_{\text{pp},0} \\
 & && \text{and to} \quad \nabla(\mathbf{u}) \geq \nabla_0 \\
 & && |\Delta B(\mathbf{u})| \leq 5\% B_0 \\
 & && |\Delta T(\mathbf{u})| \leq 5\% T_0 \\
 & && V(\mathbf{u}) \geq V_0, \\
 & && \mathbf{u}_l \leq \mathbf{u} \leq \mathbf{u}_u,
 \end{aligned} \tag{23}$$

where  $R$  is the resistance in calm water at Froude equal to 0.28,  $L_{\text{pp}}$  is the length between perpendicular,  $\nabla$  the displacement,  $B$  the overall beam,  $T$  the draught, and  $V$  the volume reserved for the sonar in the bow dome; finally,  $\mathbf{u}_l$  and  $\mathbf{u}_u$  are the lower and upper bounds of  $\mathbf{u}$ , respectively.

The design space has been defined within the activities of the NATO Science and Technology Organization, Applied Vehicle Technology (AVT), Research Task Group (RTG) 331 on “Goal-Driven, Multi-Fidelity Approaches for Military Vehicle System-Level Design” [26]. The original design space is formed by  $M = 22$  design variables, defined by the

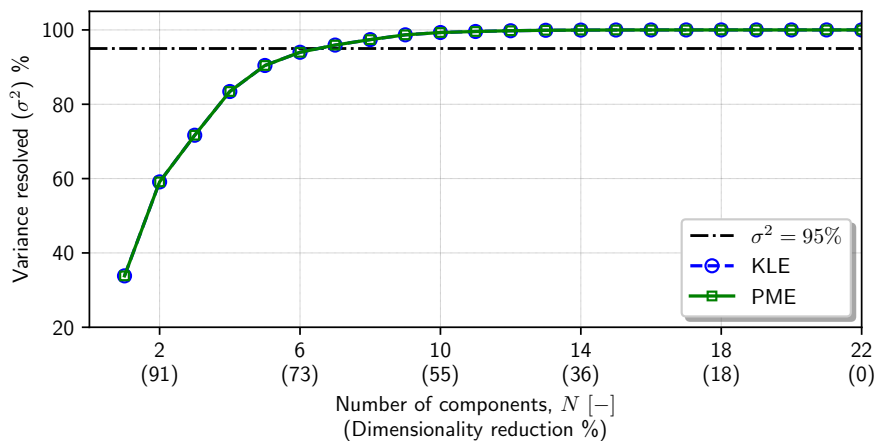


**Fig. 4 DTMB 5415 design-space dimensionality reduction: variance resolved as a function of the number of reduced design variables with KLE and PME**

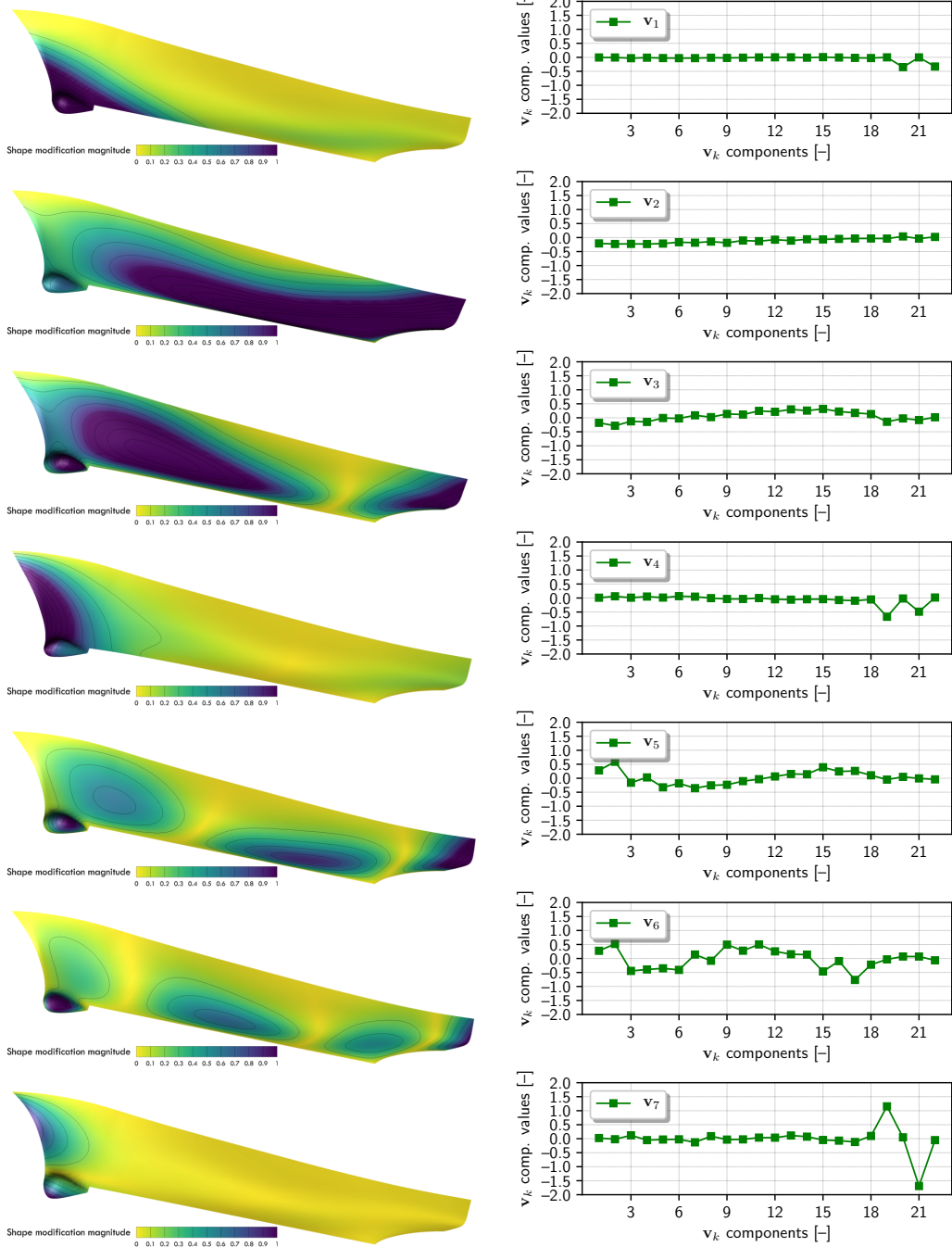


**Fig. 5 DTMB 5415 design-space dimensionality reduction: (left) the shape modification vector modes  $z_k$  and (right) modes  $v_k$  that embeds the original design variables, for  $k = 1, \dots, 7$  (from top to bottom)**

FFD method [27]. Specifically, the demi-hull is put in a lattice of  $9 \times 3 \times 3$  nodes in the  $\xi_1 \xi_2 \xi_3$  reference system, Fig. 3. Note that the FFD lattice perfectly fit the demi-hull maximum dimension. Only 21 nodes are active (see blue sphere in Fig. 3). Further details on the FFD parameterization can be found in [23].

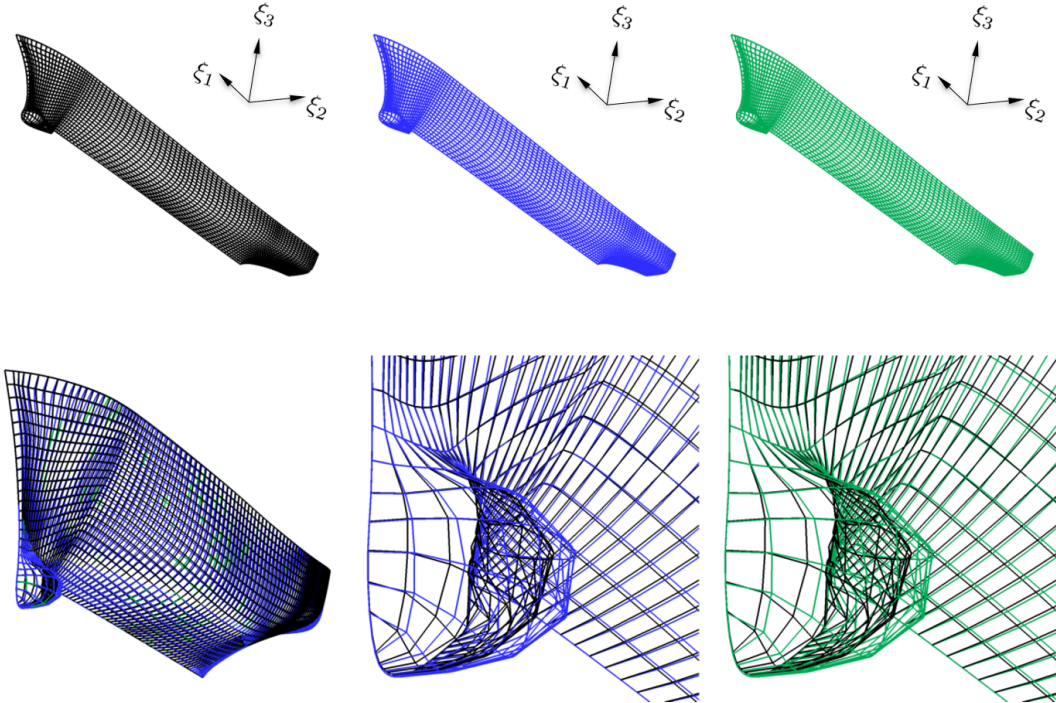


**Fig. 6 DTMB 5415 design-space dimensionality reduction: example of reconstruction of a geometry of the data set D; (top) design variant (left), reconstruction via KLE modes (center), and reconstruction via PME (right); (bottom) shapes superposition and a detail of the sonar-dome differences**

#### A. Design-space dimensionality reduction results

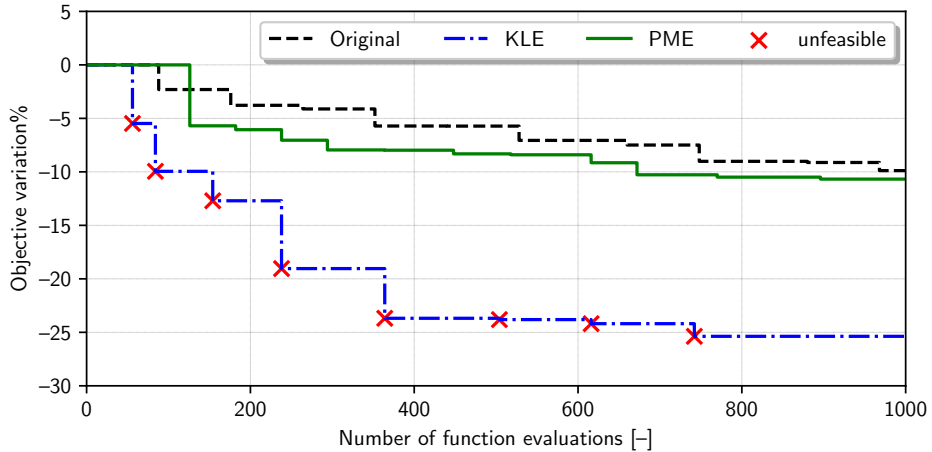
The PCA is trained by a set of  $S = 1000$  MC items [28]. For the sake of simplicity, in the following, KLE refers to the dimensionality reduction based on the shape modification vector only, whereas PME refers to the dimensionality reduction using both the shape modification and the design variables vectors. The geometry is discretized by  $90 \times 25$  grid nodes (shown with red circle in Fig. 3,  $L = 2250$ ), providing a data matrix  $\mathbf{P}$  of dimension  $[6772 \times 1000]$ . A weight coefficient  $\rho_i = 1$  (see Eq. 16) is imposed for all the grid nodes below the water line, while a null weight ( $\rho_i = 0$ ) is used for the nodes above.

Figure 4 shows the variance resolved by KLE and PME. KLE and PME cumulative sums of the eigenvalues (as percentage of the total variance) perfectly coincide. The number of reduced design variables to retain at least the 95% of the original geometric variance is equal to  $N = 7$ , achieving a dimensionality reduction close to 70%. The corresponding eigenvectors  $\mathbf{z}_k$ , that can be used as shape modification basis by KLE, are shown in Fig. 5 (left). Note that the PME method provides exactly the same eigenvector components for the shape representation, but in addition provides also the basis functions  $\mathbf{v}_k$  that embed the original design variables (see Fig. 5, right), allowing to use original shape modification method/parameterization without the need of using the geometrical eigenvectors  $\mathbf{z}_k$ .

An example of geometry reconstruction is shown in Fig. 6. Specifically, Fig. 6 (top) shows one of the 1000 MC items in  $\mathbf{D}$  obtained with FFD, KLE, and PME, from left to right, respectively and they are superposed in Fig. 6 (bottom left). Minor differences can be seen comparing the FFD (black) with KLE (blue) and PME (green) and a detail of sonar dome is provided in Fig. 6 (bottom center and right). KLE in blue and PME in green show the same reconstruction error due to the truncation of the eigenvector expansion up to  $N$  (see Eqs. 6 and 22, respectively).

#### B. Optimization results

The solution of problem in Eq. 23 is obtained with a memetic version (hybrid global/local) [29] of the deterministic particle swarm optimization algorithm [30], allowing for a total computational budget of 1000 function evaluations. The optimization are conducted in the original design space, as well as using KLE and PME reduced design spaces. The objective function is evaluated by a potential flow solver, developed at CNR-INM, whose details can be found in [31]. Specifically, using Dawson (double-model) linearization [32], the resistance of the ship is evaluated as the sum of wave



**Fig. 7 DTMB 5415 optimization: comparison of the optimization convergence within original, KLE, and PME design spaces.**

and friction components: the former is evaluated by a standard pressure integral, whereas the latter is estimated using a flat-plate approximation, based on the local Reynolds number. Simulations are performed at even keel condition for the demi-hull only, taking advantage of symmetry about the  $\xi_1\xi_3$ -plane. The computational domain for the free-surface is defined within  $0.5L_{pp}$  upstream,  $1.5L_{pp}$  downstream, and  $1L_{pp}$  sideways. The same nodes ( $90 \times 25$ ) used for the dimensionality reduction procedure (see red circle in Fig. 3) are used for the hull grid, whereas  $75 \times 22$  nodes are used for the free-surface discretization.

Figure 7 shows the optimization convergence. The optimization performed in the reduced design spaces outperforms the optimization procedure in the original design space. It may be noted how the optimization in the KLE design space (see blue dash-dotted line in Fig. 7) provides the best objective improvement, nevertheless all the optimal designs found during the optimization-algorithm evolution fall outside the original design bounds (see red cross Fig. 7). This means that the KLE domain extends beyond the original FFD bounds, thus making the comparison unfair at least for the current application. PME on the one hand spans the same KLE space while on the other hand allows for easy penalization of unfeasible designs, effectively confining the optimization process within the original design bounds. In summary, PME provides a faster convergence towards a better optimum, compared to the optimization in the original FFD design space.

## V. Airfoil Aerodynamics Problem

The problem assesses the shape reparameterization and optimization of the RAE-2822 airfoil by PME only. The operating conditions of the airfoil are Mach equal to 0.734 and Reynolds equal to  $6.5 \times 10^6$ , and the design optimization problem definition is the following:

$$\begin{aligned}
 & \text{minimize} && C_D(\mathbf{u}) \\
 & \text{subject to} && C_L(\mathbf{u}) = 0.824 \\
 & && \text{and to} \quad -0.11 \leq C_M \leq -0.01 \\
 & && t/c = 0.1211 \\
 & && r \geq 0.007c \\
 & && \tau \geq 5^\circ \\
 & && t_{85}/c \geq 0.02 \\
 & && \mathbf{u}_l \leq \mathbf{u} \leq \mathbf{u}_u,
 \end{aligned} \tag{24}$$

where  $C_D$  is the drag coefficient and  $c$  is the airfoil chord. The constraint on lift coefficient ( $C_L$ ) is satisfied using the angle of attack  $\alpha$  as a free parameter and is automatically handled by the flow analysis driver. In the proposed design problem, constraints are imposed on pitching moment  $C_M$ , maximum thickness to chord ratio  $t/c$ , leading edge radius  $r$ , trailing edge angle  $\tau$ , and thickness at 85% of the chord  $t_{85}/c$ . The constraint on the maximum thickness is automatically satisfied by the shape handler by scaling the airfoil after its parametric modification.

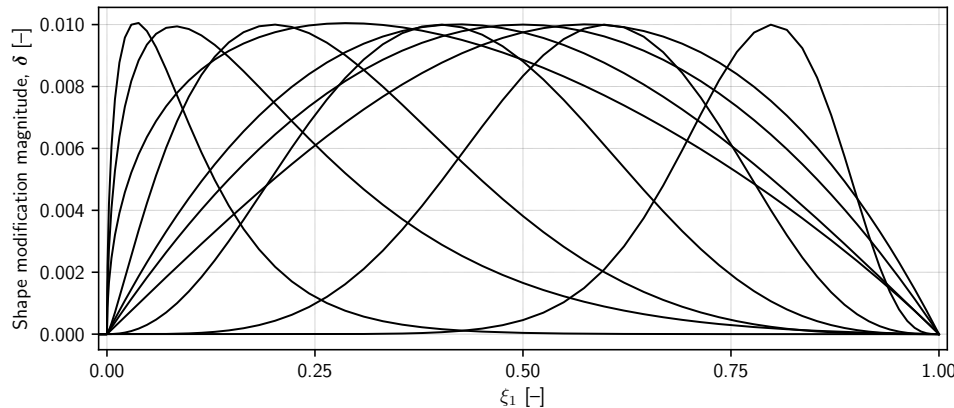


**Fig. 8 RAE-2822 problem: shape modification functions**

The design space has been defined within the activities of the NATO-AVT-331 [26] and is composed by 20 design variables, each linked to a different shape function (see Fig. 8) that operates either on upper or lower side of the airfoil [33]. Namely, the shape modification functions include 6 polynomials, 12 Hicks-Henne bumps, and 2 Wagner functions [34]. A in-house code (WG2AER developed at CIRA) parameterizes the airfoil as a linear combination of the parent geometry and the modification functions. Further details on the shape modification functions can be found in [35].

#### A. Design-space dimensionality reduction results

The PME is trained by a set of  $S = 4000$  MC items. The geometry is discretized by  $L = 364$  grid nodes, providing a data matrix  $\mathbf{P}$  of dimension  $[748 \times 4000]$ . Figure 9 shows the variance resolved by PME. The number of reduced design variables to retain at least the 95% of the original geometric variance is equal to  $N = 5$ , achieving a dimensionality reduction equal to 75%, whereas  $N = 8$  reduced-design variables, corresponding to a dimensionality reduction equal to 60%, are needed to retain at least the 99% of the original geometric variance. The corresponding eigenvectors  $\mathbf{z}_k$  and  $\mathbf{v}_k$  (for  $k = 1, \dots, 8$ ) are shown in Fig. 10. Note that the PME eigenvector components for the shape representation  $\mathbf{z}_k$  (see Fig. 10 left) are those obtained by lower and upper bound of  $\beta$  (see Eq. 21). These are not used for the shape modification in reduced design space, that is based on  $\mathbf{v}_k$  (see Fig. 10 right) through the reconstruction of the original design variables via Eq. 22, but allows to understand what are the maximum allowable deformations with the reduced-design variables.

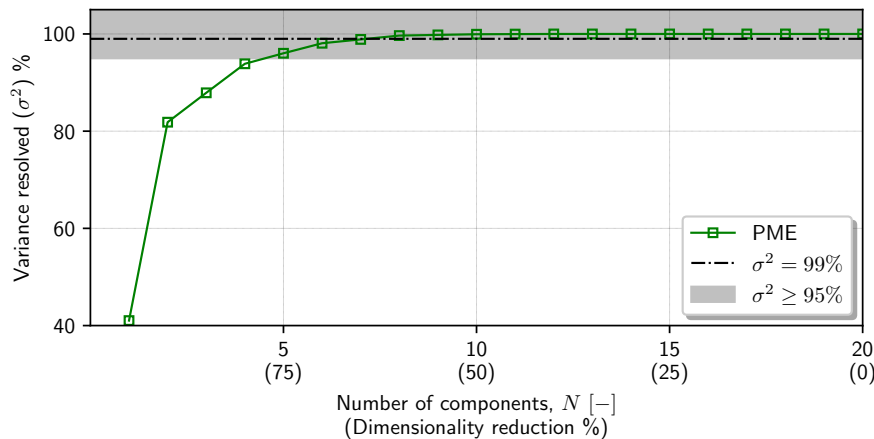


**Fig. 9 RAE-2822 design-space dimensionality reduction: variance resolved as a function of the number of reduced design variables with PME**

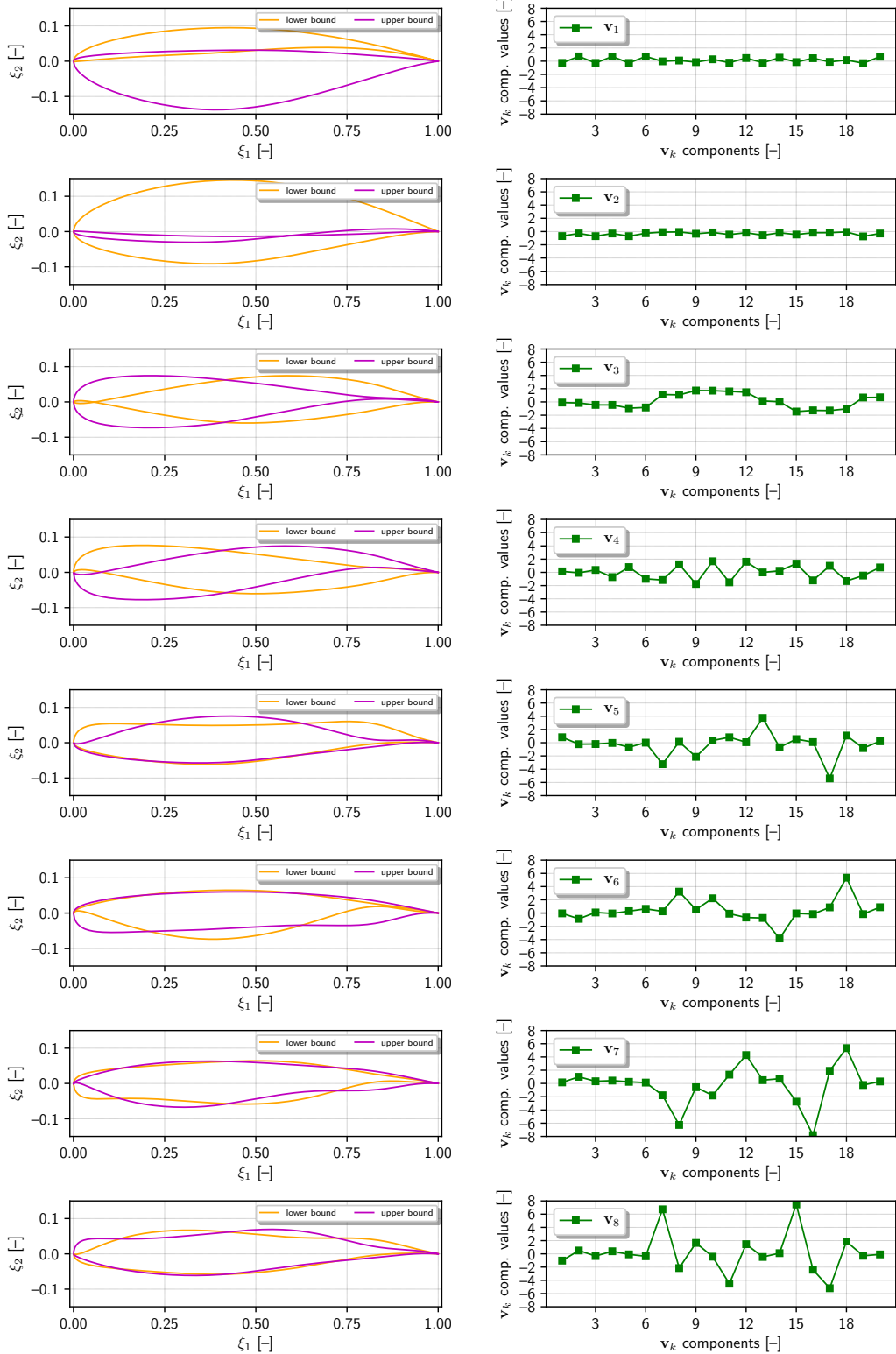


**Fig. 10 RAE-2822 design-space dimensionality reduction: (left) the shape modification vector modes  $z_k$  and (right) modes  $v_k$  for  $k = 1, \dots, 8$  (from top to bottom).**

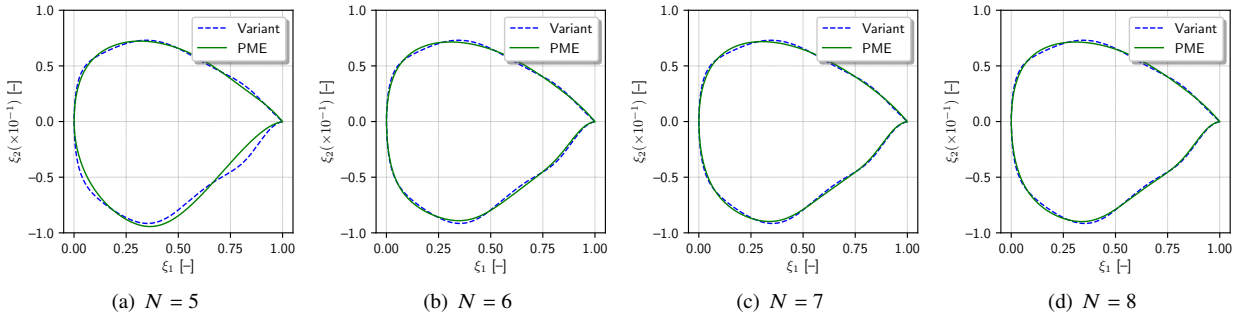


**Fig. 11 RAE-2822 design-space dimensionality reduction: example of PME reconstruction of one foil variant, conditional to the number of reduced design variables  $N$ .**

An example of geometry reconstruction is shown in Fig. 11, conditional to the number of reduced-design variables  $N$ . Specifically, one variant of the 4000 MC items in  $\mathbf{D}$  obtained with original shape parameterization and its reconstruction via PME is provided: from left to right the PME reconstruction improves, as expected, with increasing  $N$ . It can be noted that  $N = 5$  shows some evident differences, even if it sufficient to describe at least the 95% of the original design variability. If a better reconstruction is sought after,  $N = 6$  provides already a good compromise, for this specific case.

## B. Optimization results

The solution of problem in Eq. 24 is obtained with the covariance matrix adaptation evolution strategy (CMA-ES) algorithm [36], considering a total computational budget of 1000 function evaluations. The optimization are conducted in the original design space, as well as using the PME reduced design spaces with  $N = 5, \dots, 8$ . The objective function is evaluated by the open-source finite-volume code SU2 v6.2.0, a RANS equation solver developed at Stanford university, whose details can be found in [37]. Herein, the Spalart-Allmaras turbulence model [38] is used along with a 2nd-order monotone upstream-centered scheme for conservation law, and an adaptive Courant–Friedrichs–Lewy number. A circular computational domain with a radius equivalent to  $40c$  is used and it is generated GMSH v4 software [39]. The computational grid is hybrid: specifically, a structured layer of about 57k grid points is used for the boundary layer in order to guarantee a  $y^* < 1$  and an unstructured grid of about 97k points is used outside of the boundary layer, for a total of about 155k grid points. The same nodes used for the dimensionality reduction procedure are used for the boundary layer grid. Details on grids convergence studies can be found in [33].

Figure 12 shows the optimization convergence. The optimization performed in the reduced design spaces outperforms using  $N = 5$  and 6 does not allow to achieved a better optimum compared to the optimization procedure conducted in

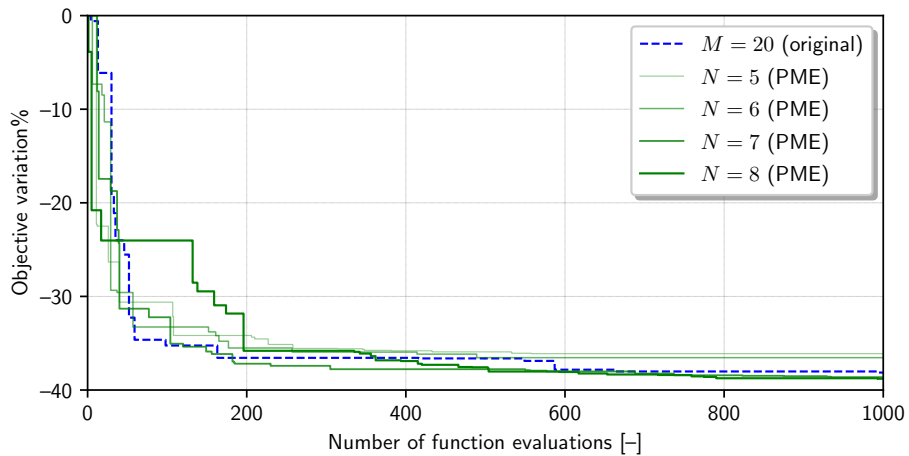


**Fig. 12 RAE-2822 optimization convergence.**

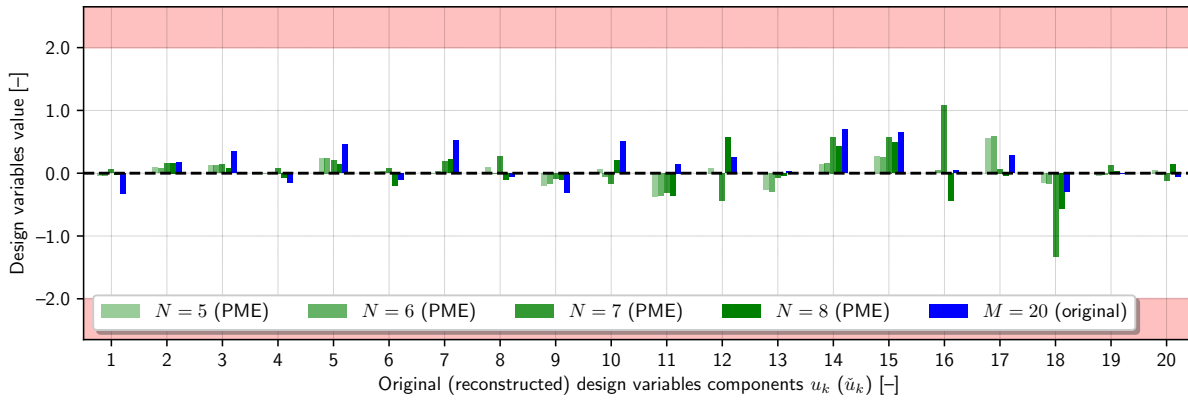


**Fig. 13 RAE-2822 optimization: comparison of optimal design variable values.**

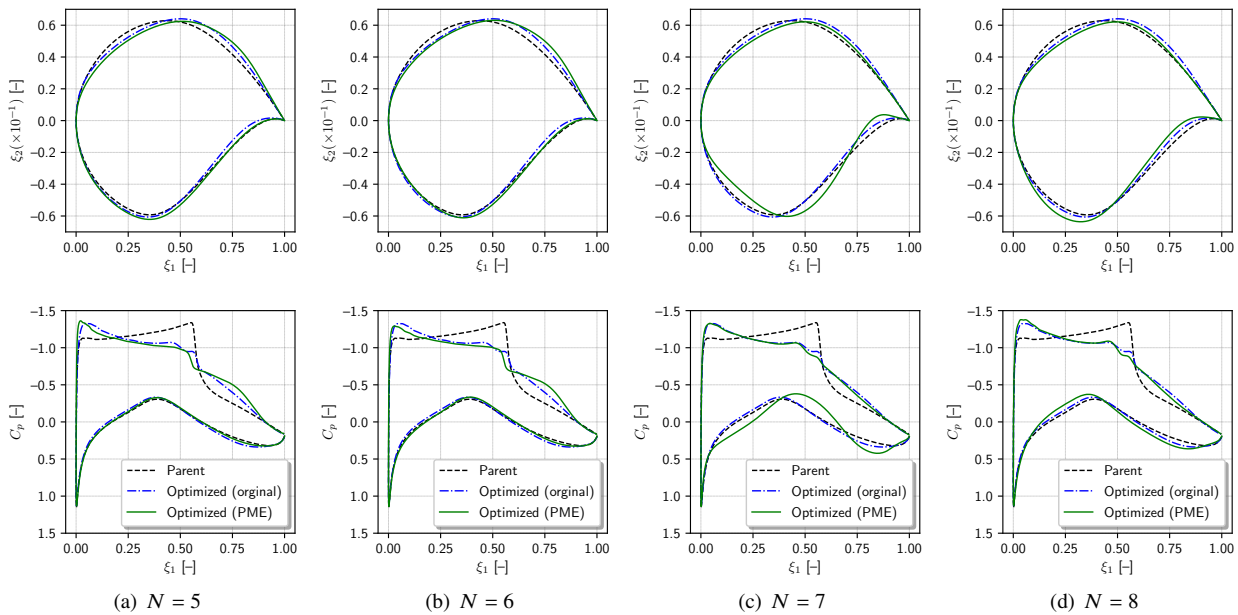


**Fig. 14 RAE-2822 optimization: airfoil shape (top) and associated pressure coefficient (bottom) comparison between parent and optimized foils in the original and reduced design space (from left to right, increasing the geometrical variance retained).**

the original design space. On the contrary, using  $N = 7$  and  $8$  better optima are found. These last two design space allow also for faster convergence towards the optimum, compared to the original design space. In particular,  $N = 7$  provides the best compromise between objective function improvement and effectiveness in achieving it. The optimal (original) design variables are compared in Fig. 13, while the associated airfoil shapes and pressure coefficient  $C_p$  along the cord are shown in Fig. 14. The optimal design variables (see Fig. 13) are quite different, but not so far from the parent foil. Indeed, the differences in the optimal shapes (see Fig. 14 top) are not highly appreciable, specially comparing  $M = 20$  to  $N = 5$  and  $6$ . Major differences are visible for  $N = 7$  and  $8$ , compared to  $M = 20$  and this justify the objective function improvement. Finally, looking both to the  $C_p$  and the Mach field (shown in Fig. 15) it can be seen that all the optimal design have reduced the shock present on the parent foil and this is definitely smoother for  $N = 7$  and  $8$  designs, compared to the others.

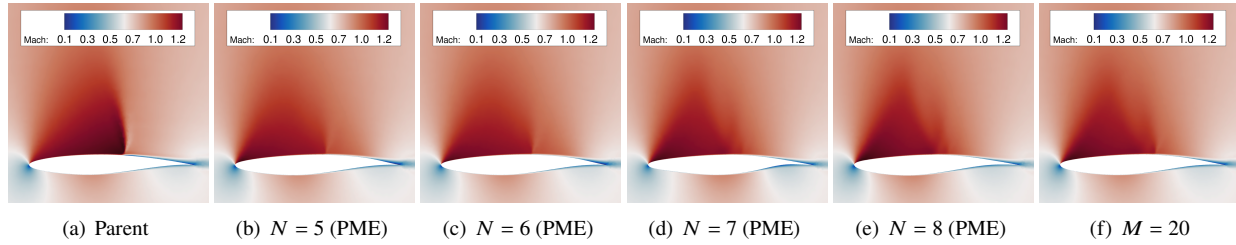


**Fig. 15 RAE-2822 optimization: Mach field comparison between parent and optimized foils.**

## VI. Conclusions and Future Work

A methodology to address the curse of dimensionality in shape optimization and improve the effectiveness and efficiency of global optimization methods has been presented. The parametric model embedding (PME) has the capability of achieving the same results of other representation learning methods, based on KLE/POD/PCA in terms of design-space assessment and dimensionality reduction, but, in addition, it provides a basis to embed directly the original design variables. This last point has a notable industrial implication, because it overcomes one of the limitations associated to the original KLE/POD/PCA formulation, i.e., the difficulty in returning to the original parameterization. PME provides the pathway for a possible direct integration in CAD software and simulation-driven design optimization tool-chains, avoiding the necessity to implement a new shape modification method based on the geometric component of the KLE/POD/PCA eigenvectors. This allows the designer to explore the reduced design with the guarantee of confining the global optimization method within the bound of the original design space, thus avoiding possible unfeasibilities of finding an optimum that not satisfies design requirements.

PME capabilities have been shown for the design optimization of destroyer-type vessel and a transonic airfoil, demonstrating its ability to provide a reduced dimensionality representation of the original design parameterization, using the original design parameters, allowing also for a faster optimization convergence towards a better optimum compared with the original design space.

Future work will investigate the possible extension of PME to physics-informed [40, 41] and physics-related formulations [42, 43], as well as to nonlinear dimensionality reduction methods [44] to overcome the limits of the linearity approximation of KLE/POD/PCA, that could not be as much efficient when strong nonlinearities are present in the shape parameterization or in the physics considered.

## Acknowledgments

The work is conducted in collaboration with the NATO task group AVT-331 on “Goal-driven, multi-fidelity approaches for military vehicle system-level design”. CNR-INM authors are grateful to the US Office of Naval Research Global for its support through grants N62909-11-1-7011 and N62909-21-1-2042. The work carried out by CIRA is supported within the internal project OPTIWING (OPTImization for WING Generation).

## References

- [1] Bellman, R. E., et al., “Dynamic programming,” *Cambridge Studies in Speech Science and Communication. Princeton University Press, Princeton*, 1957.
- [2] Serani, A., Stern, F., Campana, E. F., and Diez, M., “Hull-form stochastic optimization via computational-cost reduction methods,” *Engineering with Computers*, Vol. 38, No. 3, 2022, pp. 2245–2269.
- [3] Montgomery, D. C., and Weatherby, G., “Factor screening methods in computer simulation experiments,” Tech. rep., Institute of Electrical and Electronics Engineers (IEEE), 1979.
- [4] Sobol, I. M., “Global sensitivity indices for nonlinear mathematical models and their Monte Carlo estimates,” *Mathematics and computers in simulation*, Vol. 55, No. 1-3, 2001, pp. 271–280.
- [5] Bengio, Y., Courville, A., and Vincent, P., “Representation learning: A review and new perspectives,” *IEEE transactions on pattern analysis and machine intelligence*, Vol. 35, No. 8, 2013, pp. 1798–1828.

- [6] Diez, M., Campana, E. F., and Stern, F., “Design-space dimensionality reduction in shape optimization by Karhunen–Loève expansion,” *Computer Methods in Applied Mechanics and Engineering*, Vol. 283, 2015, pp. 1525–1544.
- [7] Li, J., Du, X., and Martins, J. R., “Machine learning in aerodynamic shape optimization,” *Progress in Aerospace Sciences*, Vol. 134, 2022, p. 100849.
- [8] Poole, D., Allen, C., and Rendall, T., “High-fidelity aerodynamic shape optimization using efficient orthogonal modal design variables with a constrained global optimizer,” *Computers & Fluids*, Vol. 143, No. Supplement C, 2017, pp. 1 – 15.
- [9] Cinquegrana, D., and Iuliano, E., “Investigation of adaptive design variables bounds in dimensionality reduction for aerodynamic shape optimization,” *Computers & Fluids*, Vol. 174, 2018, pp. 89–109.
- [10] Yasong, Q., Junqiang, B., Nan, L., and Chen, W., “Global aerodynamic design optimization based on data dimensionality reduction,” *Chinese Journal of Aeronautics*, Vol. 31, No. 4, 2018, pp. 643–659.
- [11] Allen, C. B., Poole, D. J., and Rendall, T., “Wing aerodynamic optimization using efficient mathematically-extracted modal design variables,” *Optimization and Engineering*, Vol. 19, No. 2, 2018, pp. 453–477.
- [12] Yanhui, D., Wenhua, W., Zhang, P., Fulin, T., Zhaolin, F., Guiyu, Z., and Jiaqi, L., “Performance improvement of optimization solutions by POD-based data mining,” *Chinese Journal of Aeronautics*, Vol. 32, No. 4, 2019, pp. 826–838.
- [13] Gaggero, S., Vernengo, G., Villa, D., and Bonfiglio, L., “A reduced order approach for optimal design of efficient marine propellers,” *Ships and Offshore Structures*, Vol. 15, No. 2, 2020, pp. 200–214.
- [14] Masood, Z., Khan, S., and Qian, L., “Machine learning-based surrogate model for accelerating simulation-driven optimisation of hydropower Kaplan turbine,” *Renewable Energy*, Vol. 173, 2021, pp. 827–848.
- [15] Tezzele, M., Salmoiraghi, F., Mola, A., and Rozza, G., “Dimension reduction in heterogeneous parametric spaces with application to naval engineering shape design problems,” *Advanced Modeling and Simulation in Engineering Sciences*, Vol. 5, No. 1, 2018, pp. 1–19.
- [16] D’Agostino, D., Serani, A., and Diez, M., “Design-space assessment and dimensionality reduction: An off-line method for shape reparameterization in simulation-based optimization,” *Ocean Engineering*, Vol. 197, 2020, p. 106852.
- [17] Harries, S., and Uharek, S., “Application of radial basis functions for partially-parametric modeling and principal component analysis for faster hydrodynamic optimization of a catamaran,” *Journal of Marine Science and Engineering*, Vol. 9, No. 10, 2021, p. 1069.
- [18] Liu, X., Zhao, W., and Wan, D., “Linear reduced order method for design-space dimensionality reduction and flow-field learning in hull form optimization,” *Ocean Engineering*, Vol. 237, 2021, p. 109680.
- [19] Çelik, C., Danışman, D. B., Khan, S., and Kakkis, P., “A reduced order data-driven method for resistance prediction and shape optimization of hull vane,” *Ocean Engineering*, Vol. 235, 2021, p. 109406.
- [20] Melati, D., Grinberg, Y., Kamandar Dezfouli, M., Janz, S., Cheben, P., Schmid, J. H., Sánchez-Postigo, A., and Xu, D.-X., “Mapping the global design space of nanophotonic components using machine learning pattern recognition,” *Nature communications*, Vol. 10, No. 1, 2019, pp. 1–9.
- [21] Torrijos-Morán, L., and García-Rupérez, J., “Design of slow-light-enhanced bimodal interferometers using dimensionality reduction techniques,” *Optics Express*, Vol. 29, No. 21, 2021, pp. 33962–33975.
- [22] Gaudrie, D., Le Riche, R., Picheny, V., Enaux, B., and Herbert, V., “Modeling and optimization with Gaussian processes in reduced eigenbases,” *Structural and Multidisciplinary Optimization*, Vol. 61, No. 6, 2020, pp. 2343–2361.
- [23] Serani, A., and Diez, M., “Parametric Model Embedding,” *Computer Methods in Applied Mechanics and Engineering*, 2022.
- [24] Diez, M., Serani, A., Campana, E. F., Volpi, S., and Stern, F., “Design Space Dimensionality Reduction for Single- and Multi-Disciplinary Shape Optimization,” *17th AIAA/ISSMO Multidisciplinary Analysis and Optimization (MA&O), AVIATION 2016*, Washington D.C., USA, June 13-17, 2016.
- [25] Grigoropoulos, G., Campana, E., Diez, M., Serani, A., Gören, O., Sariöz, K., Danisman, D., Visionneau, M., Queutey, P., Abdel-Maksoud, M., and Stern, F., “Mission-based hull-form and propeller optimization of a transom stern destroyer for best performance in the sea environment,” *MARINE VII: proceedings of the VII International Conference on Computational Methods in Marine Engineering*, CIMNE, 2017, pp. 83–94.

- [26] Beran, P. S., Bryson, D., Thelen, A. S., Diez, M., and Serani, A., “Comparison of multi-fidelity approaches for military vehicle design,” *AIAA AVIATION 2020 FORUM*, 2020, p. 3158.
- [27] Sederberg, T. W., and Parry, S. R., “Free-form deformation of solid geometric models,” *Proceedings of the 13th annual conference on Computer graphics and interactive techniques*, 1986, pp. 151–160.
- [28] Diez, M., and Serani, A., “From Uncertainty Quantification to Shape Optimization: Cross-Fertilization of Methods for Dimensionality Reduction,” *Advances in Uncertainty Quantification and Optimization Under Uncertainty with Aerospace Applications*, edited by M. Vasile and D. Quagliarella, Springer International Publishing, Cham, 2021, pp. 3–19.
- [29] Serani, A., Diez, M., Campana, E. F., Fasano, G., Peri, D., and Iemma, U., “Globally Convergent Hybridization of Particle Swarm Optimization Using Line Search-Based Derivative-Free Techniques,” *Recent Advances in Swarm Intelligence and Evolutionary Computation*, Studies in Computational Intelligence, Vol. 585, edited by X.-S. Yang, Springer International Publishing, 2015, pp. 25–47.
- [30] Serani, A., Leotardi, C., Iemma, U., Campana, E. F., Fasano, G., and Diez, M., “Parameter selection in synchronous and asynchronous deterministic particle swarm optimization for ship hydrodynamics problems,” *Applied Soft Computing*, Vol. 49, 2016, pp. 313 – 334.
- [31] Bassanini, P., Bulgarelli, U., Campana, E. F., and Lalli, F., “The wave resistance problem in a boundary integral formulation,” *Surveys on Mathematics for Industry*, Vol. 4, 1994, pp. 151–194.
- [32] Dawson, C. W., “A practical computer method for solving ship-wave problems,” *Proceedings of the 2nd International Conference on Numerical Ship Hydrodynamics*, Berkeley, 1977, pp. 30–38.
- [33] Quagliarella, D., Clark., D., Bryson, D., Beran, P. S., Thelen, A., Mainini, L., Yildiz, S., Nikbay, M., Minisci, E., Leyland, P., Serani, A., and Diez, M., “Reproducible industrial multifidelity optimization benchmark problems for air, space, and sea vehicles,” *Research workshop AVT-354 on Multifidelity methods for military vehicle design*, 2022.
- [34] Hicks, R., and Henne, P. A., “Wing Design by Numerical Optimization,” *Journal of Aircraft*, Vol. 15, No. 7, 1978, pp. 407–412.
- [35] Quagliarella, D., and Diez, M., “An open-source aerodynamic framework for benchmarking multi-fidelity methods,” *AIAA AVIATION 2020 FORUM*, 2020, p. 3179.
- [36] Hansen, N., “The CMA evolution strategy: a comparing review,” *Towards a new evolutionary computation*, 2006, pp. 75–102.
- [37] Economou, T. D., Palacios, F., Copeland, S. R., Lukaczyk, T. W., and Alonso, J. J., “SU2: An open-source suite for multiphysics simulation and design,” *Aiaa Journal*, Vol. 54, No. 3, 2016, pp. 828–846.
- [38] Spalart, P., and Allmaras, S., “A one-equation turbulence model for aerodynamic flows,” *30th aerospace sciences meeting and exhibit*, 1992, p. 439.
- [39] Geuzaine, C., and Remacle, J.-F., “Gmsh: A 3-D finite element mesh generator with built-in pre- and post-processing facilities,” *International Journal for Numerical Methods in Engineering*, Vol. 79, No. 11, 2009, pp. 1309–1331.
- [40] Serani, A., Campana, E. F., Diez, M., and Stern, F., “Towards Augmented Design-Space Exploration via Combined Geometry and Physics Based Karhunen-Lo  e Expansion,” *18th AIAA/ISSMO Multidisciplinary Analysis and Optimization Conference (MA&O)*, *AVIATION 2017*, Denver, USA, June 5-9, 2017.
- [41] Serani, A., D’Agostino, D., Campana, E. F., and Diez, M., “Assessing the interplay of shape and physical parameters by unsupervised nonlinear dimensionality reduction methods,” *Journal of Ship Research*, Vol. 64, No. 04, 2020, pp. 313–327.
- [42] Khan, S., Kaklis, P., Serani, A., and Diez, M., “Geometric moment-dependent global sensitivity analysis without simulation data: application to ship hull form optimisation,” *Computer-Aided Design*, 2022, p. 103339.
- [43] Khan, S., Kaklis, P., Serani, A., Diez, M., and Kostas, K., “Shape-supervised dimension reduction: Extracting geometry and physics associated features with geometric moments,” *Computer-Aided Design*, 2022, p. 103327.
- [44] D’Agostino, D., Serani, A., Campana, E. F., and Diez, M., “Nonlinear Methods for Design-Space Dimensionality Reduction in Shape Optimization,” *3rd International Conference on Machine Learning, Optimization, and Big Data, MOD 2017, Volterra, Italy*, 2017.